


Please cite the Published Version

Ghediri, D, Kihal, R, Chelaghmia, ML, Assaifan, AK, Banks, CE , Makhlouf, FZ, Fisli, H, Nacef, M, Affoune, AM, Foukmeniok, SM and Ponti , M (2025) Ruthenium nanoparticles doped on electrochemical activated screen-printed electrode for simultaneous determination of dopamine and paracetamol in pharmaceutical and human serum samples. *Microchemical Journal*, 215. 114186
ISSN 0026-265X

DOI: <https://doi.org/10.1016/j.microc.2025.114186>

Publisher: Elsevier

Version: Accepted Version

Downloaded from: <https://e-space.mmu.ac.uk/640440/>

Usage rights:  [Creative Commons: Attribution 4.0](https://creativecommons.org/licenses/by/4.0/)

Additional Information: This is an author accepted manuscript of an article published in *Microchemical Journal*, by Elsevier. This version is deposited with a Creative Commons Attribution 4.0 licence [<https://creativecommons.org/licenses/by/4.0/>], in accordance with Man Met's Research Publications Policy. The version of record can be found on the publisher's website.

Enquiries:

If you have questions about this document, contact openresearch@mmu.ac.uk. Please include the URL of the record in e-space. If you believe that your, or a third party's rights have been compromised through this document please see our Take Down policy (available from <https://www.mmu.ac.uk/library/using-the-library/policies-and-guidelines>)

Ruthenium nanoparticles doped on electrochemical activated screen-printed electrode for simultaneous determination of dopamine and paracetamol in pharmaceutical and human serum samples.

Dalia Ghediri ^a, Rafiaa Kihal ^{a, b} Mohamed Lyamine Chelaghmia* ^a, Abdulaziz K. Assaifan ^{c, d}, Craig E. Banks ^e, Fatima Zahra Makhlouf ^a, Hassina Fisli ^f, Mouna Nacef ^a, Abed Mohamed Affoune ^a, Serge Mbokou Foukmeniok ^g, Maxime Pontié ^g

^aLaboratory of Industrial Analysis and Materials Engineering, University May 8, 1945 Guelma, P.O.B. 401, Guelma 24000, Algeria

^bAbbes Laghrour University Khenchela, P.O.B 1252 Road of Batna, Khenchela 40004, Algeria

^cDepartment of Biomedical Technology, College of Applied Medical Sciences, King Saud University, P.O. Box 10219, Riyadh 11433, Saudi Arabia

^dKing Salman Center for Disability Research, Riyadh 11614, Saudi Arabia

^eFaculty of Science and Engineering, Manchester Metropolitan University, Chester Street, Manchester M1 5GD, UK

^fLaboratory of Applied Chemistry, University May 8, 1945 Guelma, P.O.B. 401, Guelma 24000, Algeria

^gGroup of Analysis and Processes, University of Angers, Faculty of Sciences, 2 Bd. Lavoisier 49045 Angers cedex 01 France

Abstract

A simple and highly selective electrochemical method using the commercially available screen-printed electrode electrochemically activated (ASPE) by cyclic voltammetry in 1.0 M H₂SO₄ and modified with ruthenium nanoparticles (RuNPs) was developed for the simultaneous determination of dopamine (DA) and paracetamol (PA). Changes in electrochemical behavior before and after the electrochemical activation of ASPE were studied by CV and EIS. The results have shown that the electrochemical activation of ASPE can improve the electrical conductivity, large surface area, and thus resulting in the formation of conducting RuNPs/ASPE nanocomposite. The morphologies and interface properties of the obtained RuNPs/ASPE nanocomposite were examined by FE-SEM, TEM, EDX, XRD, and AFM. Moreover, the electrochemical performances of the nanocomposite were investigated by CV, EIS and SWV methods. After optimization, the results show that CV, SWV, and EIS can effectively detect DA and PA using the fabricated sensor. For individual detection, SWV and EIS proved to be better techniques, particularly SWV, which exhibited the highest sensitivity (1.93 and 1.06 $\mu\text{A mM}^{-1} \text{ cm}^{-2}$) and the lowest detection limits (0.11 μM for DA and 0.17 μM for PA). However, for simultaneous detection, CV is more advantageous, providing the widest linear ranges (1.0–300 μM for DA and 1.0–400 μM for PA). Furthermore, the newly RuNPs/ASPE sensor showed excellent repeatability, reproducibility, stability, and selectivity. This sensor was successfully applied to measure PA and DA in both human blood and pharmaceutical formulations with satisfactory recovery.

Keywords: Electrochemically activated screen-printed graphite sensor; Dopamine; Paracetamol; Simultaneous determination; pharmaceutical formulations; Newborn disability

1. Introduction

Dopamine (3, 4-dihydroxyphenylethylamine; DA), is a catecholamine neurotransmitter derived from the decarboxylation of L-dopa [1]. It is widely existed in the mammalian central nervous system [2,3]. DA, also known as the "happy hormone," is essential for human emotions and cognitive functions [4]. It has a significant impact on people's behavior, such as keeping them motivated, and concentrated. Furthermore, DA is important for the function of renal, cardiovascular, central nervous and hormonal systems of mammals [5].

DA concentrations found in human bodily fluids typically range from 0.01 to 1.0 μM and are below the upper reference limit (URL, 3.3 $\mu\text{mol}/24\text{h}$) in adult urine [6]. Extremely insufficient DA levels can lead to disability related diseases, such as, Parkinsonism, schizophrenia, and Alzheimer's diseases [7]. As a result, it is required to determine DA concentration at the physiological level. Paracetamol (PA) is commonly referred as N-acetyl-p-aminophenol, tylenol or 4-acetaminophen [8]. It is characterized by its ability to reduce fever, relieve various types of pain, including muscular aches, toothaches, migraines, backache, arthritis, tension and post-operative pain, as well as relieve coughs and colds symptoms, owing to its antipyretic and analgesic properties [9,10].

In addition, when taken at therapeutic levels, PA is a highly effective healthcare solution. However, overuse of PA (4.0 g/daily) leading to serious diseases, including hepatotoxicity and nephrotoxicity, and inflammation of the pancreas [11]. Therapeutic PA concentration in plasma ranges from 10 to 25 $\mu\text{g}/\text{mL}$, whereas its toxicity concentration exceeds 200 $\mu\text{g}/\text{mL}$ (about 1.33 mM). [12–14]. Hence, N-acetylcysteine, is an effective treatment for paracetamol overdoses and can be taken as needed. Thus, determining PA is critical to ensuring human health in pharmaceutical dosages and human fluids [15, 16].

Currently, significant studies have indicated that pregnant women's use of paracetamol or dopamine, individually or in combination, can have a direct impact on newborns. These compounds are linked disability to several health issues in infants, notably neurological developmental disorders and metabolic imbalances [17–20]. These findings highlight the critical importance of monitoring and controlling the dosage of these two medications in pregnant women in order to avoid potential dangers to the fetus' and the newborn's health.

To address these issues, various techniques have been employed to detect DA and PA in biological samples, as well as waters or pharmaceutical preparations, including fluorescence spectrometry [21], chemiluminescence [22], capillary electrophoresis [23], high-performance liquid chromatography [24], colorimetric methods [25] and electrochemical sensing methods [21–27]. Among them, electrochemical sensing is considered the best technique due to their

various advantages, comprising high selectivity and sensitivity, portability, low cost and time effectiveness, simplicity, excellent reliability, accuracy and particularly a low detection limit [28, 29].

Nowadays, special attention has been given to screen-printed electrodes (SPEs) for the fabrication of electrochemical sensors in the field of electroanalysis, owing to their several advantages, such as inexpensiveness, portability, rapid response, flexibility, and widespread availability [30–33]. Portable SPEs are composed of three types of electrodes; working, counter and pseudo-reference electrodes. The most crucial is the working electrode, which can be created by printing different conductive inks onto various plastic or ceramic substrates [34]. Compared to solid carbon electrodes, SPEs are highly versatile, offering flexibility in broad material compatibility, modification possibilities, design, mass-production, and highly reproducible sensors [35]. After their single-use, it may be easily replaced after each measurement.

In addition, the graphite surface of the working electrode enables versatile surface modification using various techniques, including electrochemical treatment. This electrochemical treatment allow for the *in situ* easy activation of SPEs, significantly enhancing their surface properties [36]. As a result, the sensor exhibits improved sensitivity, stability, and reactivity, making it more efficient and reliable for detecting target analytes.

Moreover, SPEs surface modification with various nanomaterials, especially noble metals, such as Au [37, 38], Pt [39], Pd [40], and Ru [41], via electrochemical synthesis is an excellent way to boost its active surface area and improve its electrocatalytic performances, resulting an electrochemical sensors that are highly sensitive and selective for target analytes.

Thus, Ru is cheaper than other Pt-group metal compounds, such as Pt, Pd, Ir or Rh. Therefore, it appeared, early, as a convenient organic reactions catalyst [42].

In addition, Ru has different oxidation states, allowing it to form various chemical complexes with a wide range of possible uses, including but not limited to drug delivery and sensors [43]. Recently, ruthenium particles, their complexes and oxides have gained increasingly interest in organic compounds determination, particularly in the development of pharmaceutical sensors. This is due to their advantageous properties, including high electrocatalytic activity and excellent conductivity, remarkable stability, and biocompatibility [44]. Liu *et al.* used only a single step for the electrochemical deposition of Ru/NiFe-LDH-MXene onto SPE for the successful detection of nitrofurantoin. Nitrofurantoin is the active substance of a widely administrated treatment against bacterial infections. The prepared sensor exhibit excellent sensitivity and stability [45]. In the same context, another study carried out by

Ikram *et al.* reported that the detection of sulfonamide; another widely used antibiotic, has been considerably enhanced by Ru nanoparticles decoration of V@WO₃ nanocomposite [46]. Prabhu *et al.* incorporated Ruthenium-doped TiO₂ and reduced graphene oxide (rGO) into a carbon paste electrode (CPE) for sensitive and selective fungicide detection in soil, water, vegetables, and fruits. Fungicides are chemical compounds that serve as biocides, disinfectants, and preservatives [47].

However, only a few papers have reported the electrochemical sensing of dopamine and paracetamol via ruthenium modified electrodes and the results are encouraging. Duraisamy *et al.* synthesized a SPE modified electrode using drop coating of a ruthenium doped vanadium carbide. The sensor exhibited a very low limit of detection of 0.024 μ M and was successfully tested for paracetamol determination in drug and human blood samples [48]. Abdelwahab *et al.* developed ruthenium nanoparticles (RuNPs) uniformly anchored on chemically treated graphene oxide nanosheets (CTGONS). The resulting sensor exhibited excellent performance for the simultaneous detection of dopamine and paracetamol in human serum [49].

In this study, and to the best of our knowledge, we report for the first time the use of SPEs that were electrochemically activated in 0.1 M H₂SO₄, and subsequently decorated with ruthenium nanoparticles via a simple electrochemical route using the CV method, for the simultaneous detection of dopamine and paracetamol in PBS solution.

The performance of designed Ru-decorated activated SPE, electrochemical sensor for the individual and simultaneous detection of PA and DA was probed using CV, SWV and EIS in both standard and real samples. Notably, single-frequency EIS has rarely been employed in such systems, with only a few studies reported in the literature [27, 39]. The results showed that the as-fabricated, Ru-decorated activated SPE, exhibited excellent stability, reproducibility and selectivity for both voltammetric and impedimetric determination of PA and DA. Furthermore, the obtained sensor provided excellent recovery results for the simultaneous determination of PA and DA in human serum samples and pharmaceutical formulations without significant interferences.

Experimental section

1.1 Chemicals and Reagents

Ruthenium chloride (RuCl₃·3H₂O), dopamine (DA), paracetamol (PA), sulfuric acid (H₂SO₄), potassium chloride (KCl), uric acid (C₅H₄N₄O₃), sucrose (C₁₂H₂₂O₁₁), fructose (C₆H₁₂O₆), glucose (C₆H₁₂O₆), ascorbic acid (C₆H₈O₆), caffeine (C₈H₁₀N₄O₂), and potassium hexacyanoferrate (K₃Fe(CN)₆ / K₄Fe(CN)₆), were bought from Sigma-Aldrich and used

without any purification. All other reagents and solvents were of analytical grade. A phosphate buffer solution (PBS, 0.1 M) at pH 7.4 was prepared by mixing 0.1 M NaH_2PO_4 and Na_2HPO_4 . Other pH solutions ranging from 5.0 to 9.0 were adjusted using 0.5 M H_2SO_4 and 2.0 M NaOH . Double-distilled water with a resistivity of 18 $\text{M}\Omega\text{ cm}$ was used throughout the experiments. Commercial Doliprane tablets were procured from a local pharmacy and Dopamine hydrochloride injections were obtained from a local hospital.

1-2 Apparatus and electrochemical characterization

The electrochemical experiments were taken out with a potentiostat/galvanostat (Princeton Applied Research, AMETEK, USA) controlled by Versa Studio software. SPE electrode system consisting of a working electrode (3.1 mm diameter) decorated with Ru nanoparticles, graphite as a counter electrode, and silver/silver chloride as a reference electrode. The SPEs were manufactured at Manchester Metropolitan University. CV, SWV, EIS and EIS techniques were utilized to investigate the electrochemical properties and electro-catalytic performances of the modified SPEs.

CV was done by scanning the potential from -0.4 V to 0.6 V at a scan rate 50 mV/s in 0.1 M PBS solution (pH 7.4) for DA and PA. Each SWV was recorded from -0.60 to 0.20 V with the parameters as follow: step height increment 0.005 V , pulse amplitude 0.05 V , and pulse width 0.2 s . EIS was also performed at the frequency range from 100 kHz to 0.1 Hz with an amplitude of 10 mV . The working potential was optimized at 0.1 V for dopamine and 0.2 V for paracetamol. Data analysis and fitting were performed using EC-Lab software. The morphologies and the elemental composition of the as-elaborated electrodes were examined by means of a field emission gun by scanning electron microscopy (FE-SEM) using a JSM-6301 F apparatus from JEOL (Japan). The transmission electron microscopy (TEM) image was obtained by a JEOL JEM-1400 TEM (Japan). X-ray diffraction (XRD) data were acquired with a Bruker D8 Discover spectrometer (Germany) utilizing $\text{Cu-K}\alpha$ radiation ($\lambda = 1.5418$) to evaluate the crystalline structure of the modified electrodes. Atomic force microscopy (AFM) images were taken with a Nanoscope III from Bruker, Germany, to get insights into surface morphology.

1-3 Preparation of the Modified SPE with Ruthenium

Prior to ruthenium electrodeposition, the graphite surface of the SPE was electrochemically activated in 1.0 M H_2SO_4 through a two-step process. The graphite surface was polarized at a constant potential of 1.8 V for 5 minutes. After that, the surface was subjected

to cyclic polarization. The potential was swept between -0.4 V (hydrogen evolution potential) and 1.8 V (beyond oxygen evolution potential) for 50 cycles at a scan rate of 50 mV/s.

The Ru nanoparticles were deposited onto the activated working electrode surface by performing fifteen successive voltammetric cycles in a 0.1 M H_2SO_4 solution containing 1.0 mM RuCl_3 . The potential was cycled between -0.4 V and -1.2 V at a scan rate of 50 mV/s, and the process was carried out at room temperature. After the fabrication of the RuNPs/ASPE, it was rinsed with deionized (DI) water and allowed to dry at room temperature. Prior to use, the RuNPs/ASPE was conditioned by performing at least 50 cycles in the potential range from -0.4 V to 0.6 V in a 0.1 M PBS solution (pH 7.4) at a scan rate of 50 mV/s, until a stable CV response was obtained.

1-4 Samples preparation

SWV technique was used to investigate the efficiency of the RuNPs/ASPE sensor's ability to detect DA and PA from dopamine hydrochloride injections, paracetamol tablets, and human blood samples. Dopamine injectable solutions (40 mg/mL) were diluted in 10 mL of 0.1 M PBS (pH 7.4). Paracetamol sample solutions were prepared as follows: three paracetamol tablets (1.0 g/tablet) were finely crushed in an agate mortar and accurately weighed. The powder was dissolved in water using ultrasonication. After centrifugation at 3500 rpm for 20 minutes, the supernatant was filtered and transferred into a 50 mL flask, then diluted with 0.1 M PBS (pH 7.4). Additionally, the RuNPs/ASPE electrochemical sensor was tested using human blood samples obtained from healthy adults donors at a local hospital. These samples were pretreated following to the methodology described in our previous studies [50].

2. Results and Discussion

2.1 Surface Morphology of modified SPEs

The morphologies of ASPE and RuNPs/ASPE were examined using FESEM, as illustrated in Figs. 1A and 1B. The characteristic wrinkles structures of graphite were observed on ASPE (Fig. 1A), which is beneficial for providing a large surface area. After Ru modification (Fig. 1B), the graphite surface became well decorated with spherical Ru nanoparticles. TEM images (Fig. 1C) further confirm that the Ru nanoparticles were homogeneously dispersed on the modified graphite SPE, exhibiting a spherical shape with an average size of approximately 50 nm. Additionally, energy spectrum analysis of Fig. 1D confirms the presence of C, O, and Ru elements.

In order to further understand the structure and phase of as-prepared RuNPs/ASPE., X-ray diffraction (XRD) analysis was conducted. Fig.1E displays the XRD pattern of the as-modified RuNPs/ASPE. From this figure, we noticed five peaks at angular positions 26.06°, 42.82°, 44.60°, 54.23°, and 77.29°, respectively correspond to (002), (100), (101), (004), and (110) diffractions of hexagonal graphite phase (JCPDS No. 00-001-0646). Furthermore, crystalline peaks at 42.82° and 44.60° were attributed to the diffraction planes (002) and (101) of hexagonal ruthenium structure (JCPDS cards No. 00-006-0663). XRD analysis indicates the successful growth of RuNPs onto surface's ASPE.

AFM measurements were performed to investigate the surface morphology variations of activated SPE before and after Ru nanoparticles electrodeposition. As shown in the 3D images Figs. 1F and 1G, the modified electrode surfaces exhibited increased roughness, with an average roughness of 582 nm for RuNPs/ASPE compared to 427 nm for ASPE. The increased roughness of RuNPs/ASPE suggests a larger exposed surface area, which is beneficial for enhancing the electrochemical detection of DA and PA.

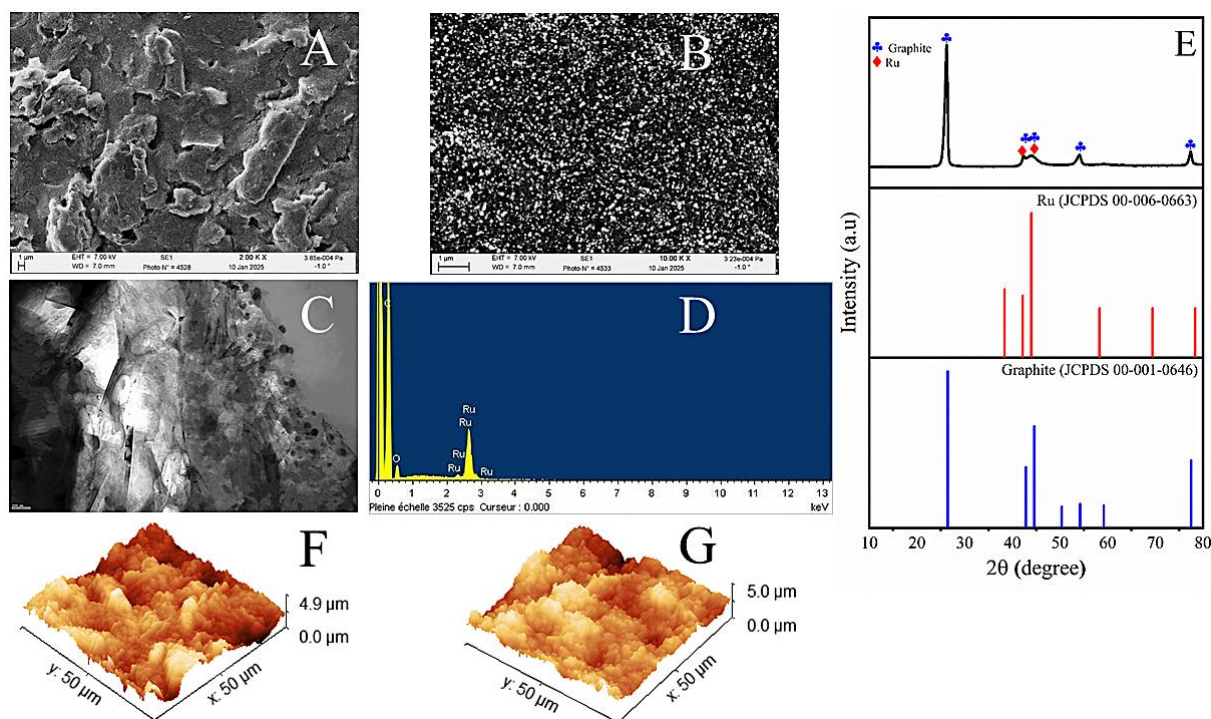


Fig. 1. FE–SEM images of ASPE (A) and RuNPS/ASPE (B); TEM images of RuNPS/ASPE (C); XRD patterns of RuNPS/ASPE (E); EDX of RuNPs/ASPE (D); 3D AFM images of ASPE (F) and RuNPs/ASPE (G)

2.2 Electrochemical characterization of the surface modified SPE

To assess the electrochemical behaviors of unmodified and modified electrodes via the ferricyanide system, CV and EIS measurements were carried out at the electrode surface using 1.0 mM $\text{Fe}(\text{CN})_6^{3-/4-}$ as a redox probe in an aqueous 0.1 M KCl solution (Fig. 2).

Fig 2A shows the CV curves of bare SPE, ASPE, and RuNPs/ASPE, respectively, obtained at a potential scan from -0.4 to 0.6 V and acquired at a fixed scan rate of 50 mV s^{-1} . As shown in this figure, the redox peak currents of RuNPs/ASPE are significantly higher compared to those of ASPE and unmodified bare SPE. These findings indicated that the SPE's modification with electrochemical activation of graphite support and Ru nanoparticles improved the electroactive surface area. The redox probe's peak-to-peak separation between the anodic and cathodic peaks (ΔE_p) increased in the following order: $109 \text{ mV} < 121 \text{ mV} < 178 \text{ mV}$ for RuNPs/ASPE, ASPE, and bare SPE, respectively. Hence, the activation of graphite and the incorporation of Ru nanoparticles onto the SPE can effectively increase the electrode surface area, improve the conductivity, and increase the electron transfer rate between the solution and electrode surface.

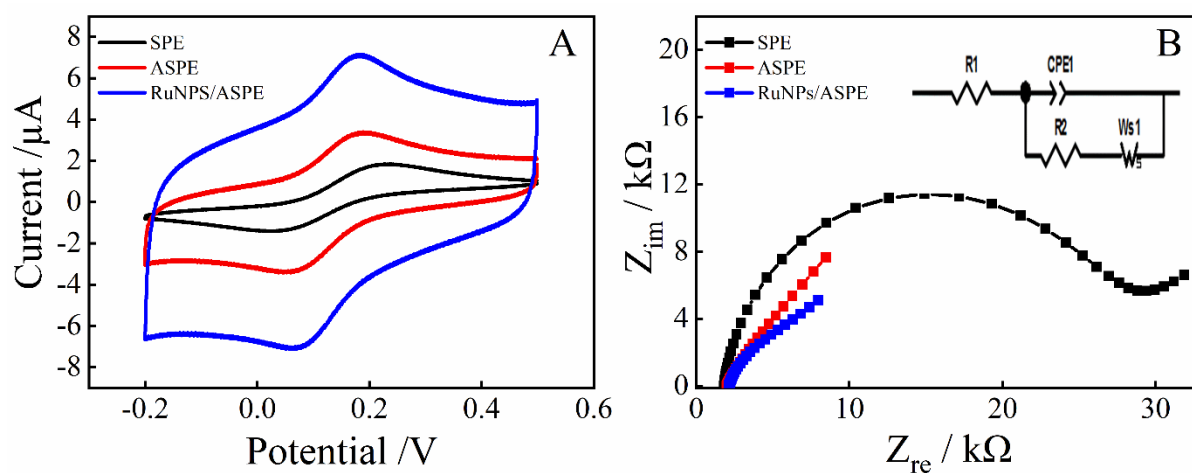


Fig. 2 (A) CV curves and (B) Nyquist plots of 1.0 mM $\text{Fe}(\text{CN})_6^{3-/4-}$ in 0.1 M KCl at unmodified SPE; ASPE and RuNPs/ASPE, scan rate 50 mVs^{-1} ; Inset (B): Randles's equivalent circuit.

To study the interface properties of unmodified and modified electrodes, EIS was also employed in the frequency ranging from 100 kHz to 0.1 Hz. Fig. 2B shows the EIS plots of bare SPE, ASPE and RuNPs/ASPE. RuNPs/ASPE with a low semi-circular diameter showed lower electron resistance and improved interfacial conduction between electrode/electrolyte compared to unmodified bare SPE and ASPE. This suggests that Ru nanoparticles reduced the electron transfer resistance and improved electron-transport efficiency.

The theoretical EIS plots were fitted to an appropriate equivalent circuit (see Fig. 2B, inset), which included the solution resistance (R_1), charge transfer resistance (R_2), warburg simulating element (WS_1), and constant phase element (CPE_1). The R_2 values for bare SPE, ASPE, and RuNPs/ASPE were found to be 25.1 K Ω ($\chi^2 = 0.044$), 11.8 K Ω ($\chi^2 = 0.046$), and 3.14 K Ω ($\chi^2 = 0.044$), respectively. Hence, the modified, RuNPs/ASPE, electrode exhibited the lowest R_2 value, indicating higher electrical conductivity than the other electrodes. These results are effectively confirmed by CV.

The electroactive surface areas of bare SPE, ASPE and RuNPs/ASPE were estimated using CV method at varied scan rates (Fig. S1), following the Randles–Sevcik formula [48]:

$$I_p = 0.436nFAC\sqrt{\frac{nFDv}{RT}}$$

where, I_p is the anodic peak current (A), A is the electroactive surface area of the working electrode in (cm^2), n is the number of exchanged electrons, C is the concentration of $\text{Fe}(\text{CN})_6^{-3/-4}$ (mol cm^{-3}), D is the diffusion coefficient of a 1.0 mM $[\text{Fe}(\text{CN})_6]^{-3/-4}$ solution containing 0.1 M KCl ($7.6 \times 10^{-6} \text{ cm}^2 \text{ s}^{-1}$), v is the scan rate (V s^{-1}).

The calculated electrochemical surface areas were 5.4×10^{-2} , 6.8×10^{-2} , and $8.79 \times 10^{-2} \text{ cm}^2$ for bare SPE, ASPE and, RuNPs/ASPE, sequentially.

2.3 Analytical performance of the RuNPs/ASPE sensor for DA and PA determination

The electrochemical behaviors of DA, PA, and their mixture were examined at unmodified and modified electrodes by CV in 0.1 M PBS (pH = 7.4) as supporting electrolyte with 100 μM of DA and PA. Fig. 3 shows the CV responses of PA and DA at unmodified SPE, ASPE, and RuNPs/ASPE in the potential range from -0.4 to 0.6 V recorded at scan rates of 50 mVs^{-1} . As seen in this figure, an almost similar response was observed across the different electrodes, and the oxidation peaks of PA and DA were completely separated without any mutual interference, regardless of the electrode type. The lowest peak value was observed on the unmodified SPE, indicating that the SPE has a slow electron transfer towards PA and DA oxidation. A higher peak current was achieved on the ASPE, proving its stronger accumulation ability compared to the unmodified SPE, due to excellent catalytic effect of the modifier layer. When the ASPE was decorated with Ru, the peak potentials of PA and DA shifted negatively, while the peak currents of PA and DA increased by 2.3 times and 1.5 times, respectively. The possible role of graphite substrate in the higher activity of RuNPs/ASPE is that OH-like functional groups on graphite (phenolic, carboxyl) participate in the oxidation of the absorbed intermediate species formed in DA and PA dissociation [37, 52].

These results indicate that RuNPs/ASPE exhibits enhanced electrocatalytic properties for the sensing of both DA and PA, compared to the other tested electrodes.

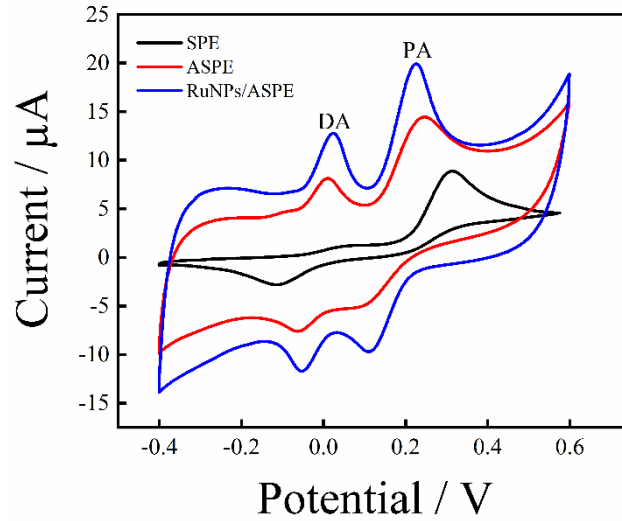


Fig. 3 CVs responses to the mixture of 100 μM PA and DA at bare SPE, ASPE, and RuNPs/ASPE in 0.1 M PBS ($\text{pH} = 7.4$), at scan rates of 50 mVs^{-1} .

2.4 Scan rate effect

Further, the mass transfer behavior of analytes at the RuNPs/ASPE was studied with CV at various scan rates ranging from 10 to 400 mVs^{-1} , with a concentration of $300 \mu\text{M}$ for both analytes. As shown in Fig. 4A, the redox peak currents of PA and DA exhibit an increase with the rise in scan rate. Additionally, a slight shift is observed in the anodic and cathodic peak potentials, moving slightly towards more positive and negative values, respectively.

Fig. 4B and 4C demonstrate an excellent linear relationship between the peak currents of DA and PA and the square root of the scan rates ($v^{1/2}$), with a high correlation coefficients, as expressed by the following equations:

$$\text{DA: } I_{pa}(\mu\text{A}) = 2.381 v^{1/2} (\text{mVs}^{-1})^{1/2} - 1.989 (R^2 = 0.998),$$

$$I_{pc}(\mu\text{A}) = -2.545 v^{1/2} (\text{mVs}^{-1})^{1/2} + 8.939 (R^2 = 0.994),$$

$$\text{PA: } I_{pa}(\mu\text{A}) = 2.294 v^{1/2} (\text{mVs}^{-1})^{1/2} - 1.444 (R^2 = 0.991),$$

$$I_{pc}(\mu\text{A}) = -1.381 v^{1/2} (\text{mVs}^{-1})^{1/2} + 5.74 (R^2 = 0.990).$$

This linearity supports a diffusion-controlled process for the electrochemical reaction of PA and DA on the surface of RuNPs/ASPE.

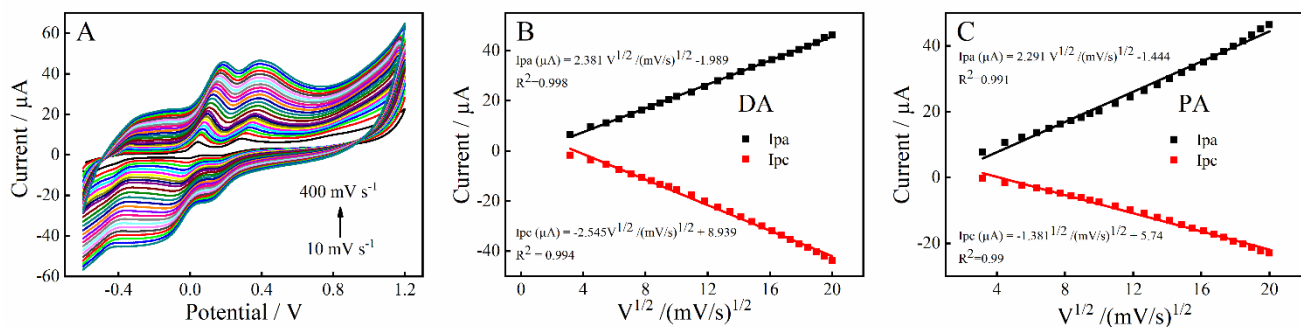


Fig. 4 (A) CVs responses of RuNPs/ASPE in the mixture of 300 μM DA and PA at various scan rates (10–400 mV s^{-1}), (B, C) dependence of peak currents of DA and PA vs. $v^{1/2}$.

2.5 Optimization of pH

The influence of pH on the electro-oxidation of 100 μM DA and 200 μM PA was investigated using CV at a RuNPs/ASPE sensor in 0.1 M PBS across various pH values, as shown in Fig.5. As the pH increased from 5.0 to 7.4, the peak currents of both analytes gradually increased, accompanied by a negative shift in peak potentials (Figs. 5A, 5B and 5C). This behavior suggests the involvement of protons in the electron transfer processes at the electrode/electrolyte interface up to pH 7.4. However, as the pH further increased from 7.4 to 10.0, the peak current decreased. This decline can be attributed to the deprotonation of the target molecules due to the higher OH^- ion concentration, leading to electrostatic repulsion between the deprotonated species and the sensor surface in an alkaline medium [53]. Therefore, a phosphate buffer electrolyte at pH 7.4, close to physiological pH, was selected as the optimal condition for the simultaneous determination of PA and DA.

In Fig. 5D, the anodic peak potentials of PA and DA shifted negatively and good linear relationships were seen as pH increased from 5.0 to 10.0. The linear relationships between E_{pa} and pH are given by: $E_{\text{pa}} (\text{V}) = -43 \text{ pH} + 647$ ($R^2 = 0.992$) for DA and $E_{\text{pa}} (\text{V}) = -56 \text{ pH} + 650$ ($R^2 = 0.992$) for PA, respectively. According to the Nernst equation, the slope values for DA and PA are 43 mV/pH and 56 mV/pH, respectively. These values are close to the theoretical value of 59 mV/pH [54], indicating an equal contribution of protons and electrons ($n = 2$) in the redox processes of both PA and DA at the RuNPs/ASPE surface. The electrode mechanism of DA a PA at RuNPs/ASPE is shown in Scheme 1. This observation aligns well with previously reported studies on the electrochemical oxidation of DA and PA using various catalysts [19, 23].

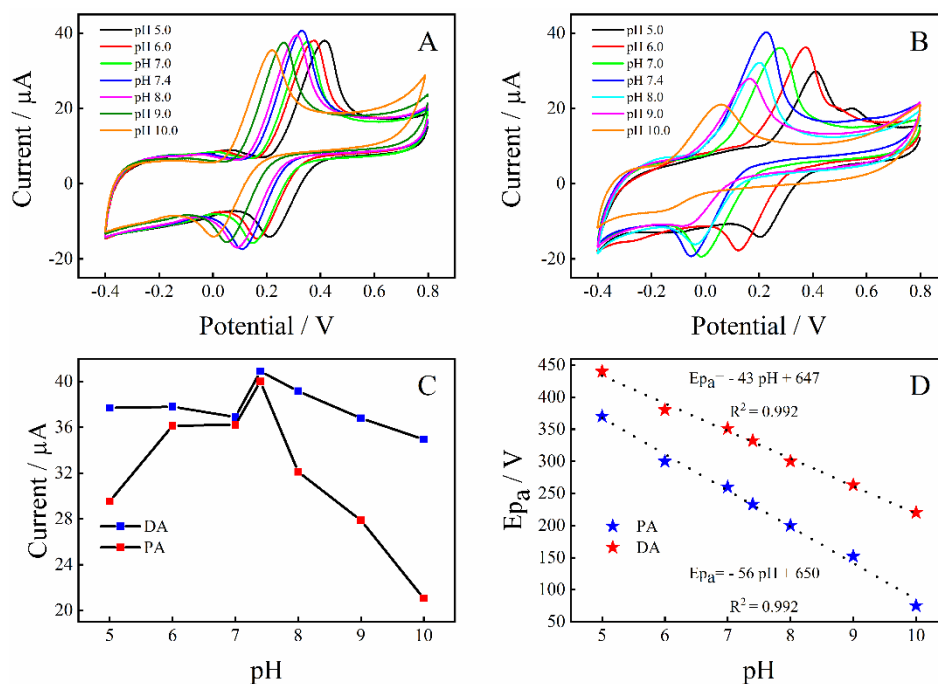
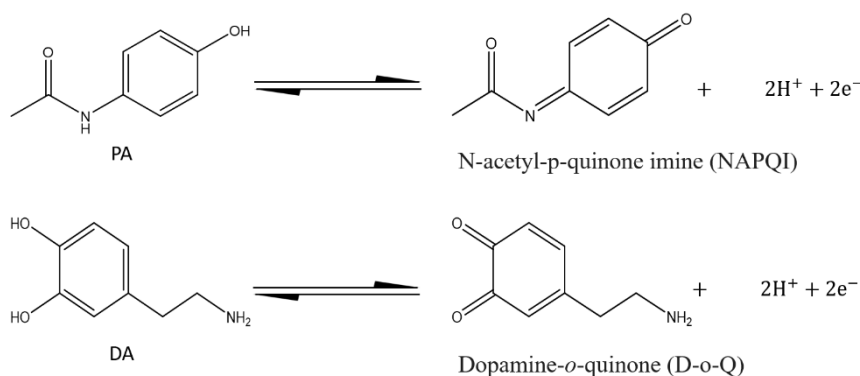


Fig. 5 CVs response of various pH values of (A) 0.1 mM DA; (B) 0.2 mM PA, at RuNPs/ASPE in 0.1 M PBS at 50 mV s^{-1} ; (C) The influence of pH on the peak current oxidation of DA and PA; (D) the plots of E_{pa} of DA and PA vs. pH



Scheme 1. Proposed oxidation mechanisms of DA and PA molecules at the surface of RuNPs/ASPE.

2.6 Electrochemical sensing behaviors at RuNPs/ASPE

To assess the sensor's sensitivity toward DA and PA, CV, EIS, and SWV measurements were employed. Initially, CV was conducted to examine the effect of varying DA and PA concentrations on the RuNPs/ASPE in 0.1 M PBS (pH 7.4) at a sweep rate of 50 mV s^{-1} , as shown in Fig. 6A and Fig. 6C, respectively. The results reveal a progressive increase in oxidation peak currents with rising DA and PA concentrations, with detectable ranges of 1.0–

300 μM for DA and 1.0–400 μM for PA. For DA, the calibration plot (Fig. 6B) exhibits two distinct linear regions. The first, ranging from 1.0 to 50 μM , follows the equation: $I_p (\mu\text{A}) = 0.141 C_{\text{DA}} (\mu\text{M}) + 6.183$ ($R^2 = 0.996$). The second extends up to 300 μM and is described by: $I_p (\mu\text{A}) = 0.055 C_{\text{DA}} (\mu\text{M}) + 10.66$ ($R^2 = 0.996$).

Similarly, the oxidation peak current of PA (Fig. 6D) exhibits two distinct linear regions: 1.0–50 μM and 50–400 μM . The corresponding regression equations are: $I_p (\mu\text{A}) = 0.076 C_{\text{PA}} (\mu\text{M}) + 3.375$, ($R^2 = 0.994$) for the lower range and $I_p (\mu\text{A}) = 0.032 C_{\text{PA}} (\mu\text{M}) + 5.943$, ($R^2 = 0.994$) for the higher range. The presence of two linear regions in both DA and PA may be attributed to the adsorption of intermediates [27]. The limit of detection (LOD), determined using a signal-to-noise ratio, was calculated as 0.8 μM for DA and 0.7 μM for PA based on the calibration curve in the lower concentration range. Additionally, the sensor's sensitivity for DA and PA detection was $1.76 \mu\text{A} \mu\text{M}^{-1} \text{cm}^{-2}$ and $0.95 \mu\text{A} \mu\text{M}^{-1} \text{cm}^{-2}$, respectively.

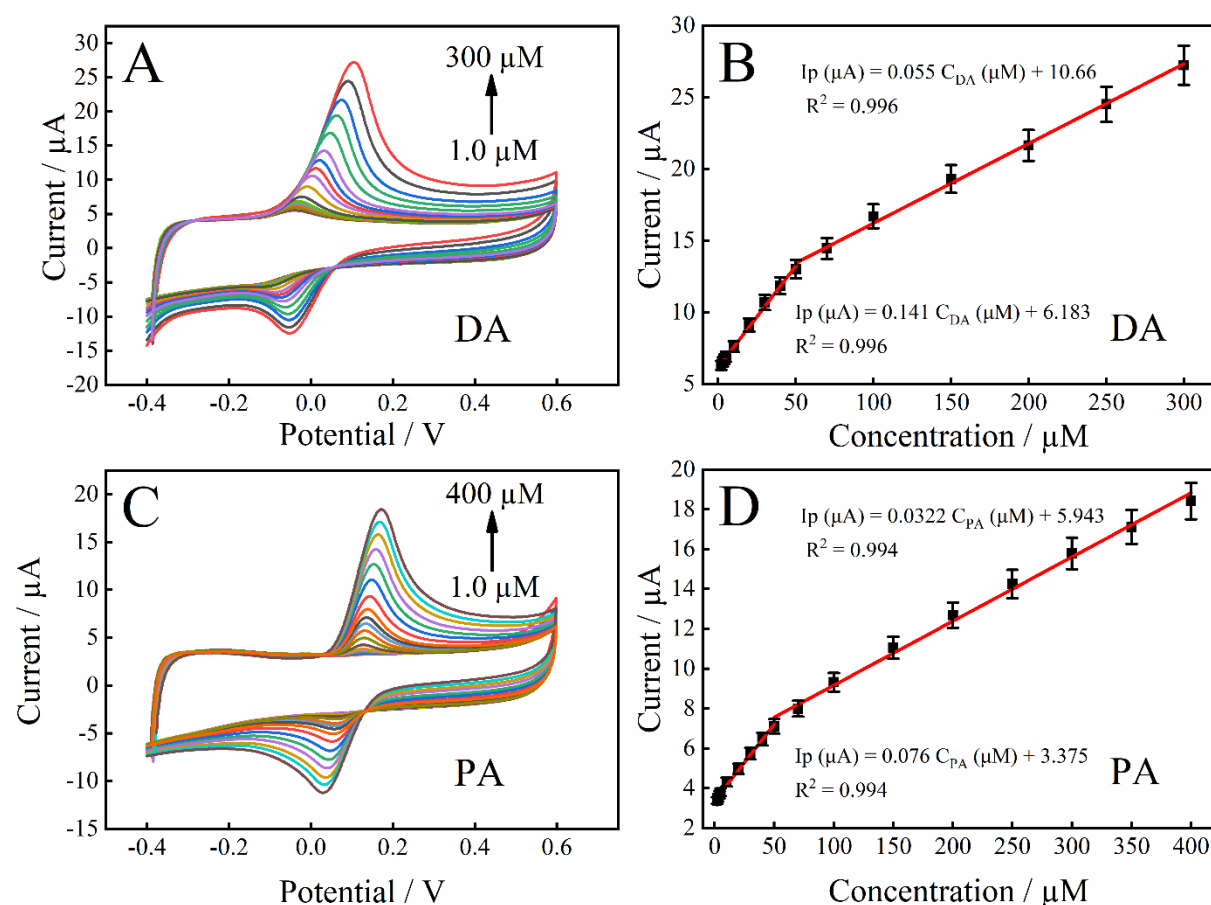


Fig. 6 CVs of different concentrations of (A) DA, (C) PA, at RuNPs/ASPE in 0.1 M PBS, scan rate 50 mV s^{-1} ; (B, D) show the dependence of I_p vs. concentration.

Similar to the CV analysis, the analytical response of DA and PA on the newly developed RuNPs/ASPE was evaluated using the EIS technique.

The corresponding Nyquist plots are shown in Fig. 7A and Fig. 7C, while the equivalent circuit and the Bode plots are shown in Supplementary content (Figs. S2, S3 and S4)

The diameter of the Nyquist semicircle decreased significantly with increasing DA and PA concentrations, indicating enhanced charge transfer. This behavior is attributed to the chemical interaction between DA or PA and the high-valence Ru species, as well as to the increased number of electroactive molecules available at the electrode surface. Both DA and PA can undergo stepwise redox reactions involving the release of $2\text{H}^+/2\text{e}^-$, thereby facilitating electron exchange between the electrode and the analytes. These findings are consistent with those reported by Motahhare Emadoddin *et al* [55].

To further assess the sensor's performance, single-frequency EIS measurements were conducted. A calibration plot was generated by plotting the relative variation of $1/Z$ as a function of DA and PA concentrations at a frequency of 0.2 Hz (Fig. 7B and 7D).

The calibration plot for DA exhibited excellent linearity over the range of 1.0–500 μM ($R^2 = 0.995$). In contrast, the calibration curves for PA displayed two distinct linear regions: 1.0–150 μM ($R^2 = 0.996$) and 150–1000 μM ($R^2 = 0.995$). The low detection limits of 0.92 μM for DA and 1.1 μM for PA further highlight the exceptional sensitivity and effectiveness of the RuNPs/ASPE as an impedimetric sensor. These results can be related to the fact that DA and PA adsorbed on the electrode surface reduce electron transfer and decreases in the amount of R_{ct} .

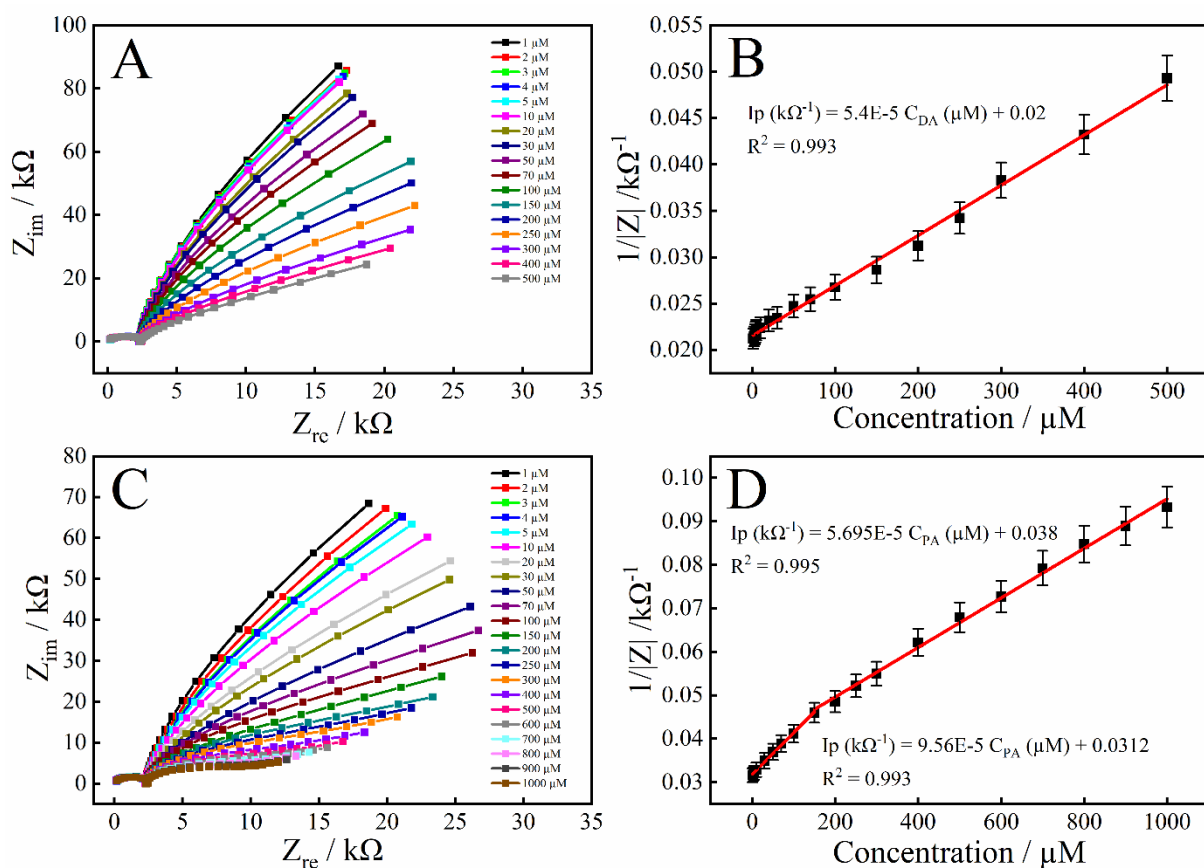


Fig. 7 Nyquist plots of RuNPs/ASPE with subsequent injections of (A) DA, (C) PA concentrations in 0.1 M PBS; (B, D) Plots of $1/|Z|$ vs. concentration.

Additionally, the individual SWV response for each analyte was investigated while maintaining the other one at a fixed concentration (Fig. 8A–D).

Fig. 8A presents the SWV profiles of the RuNPs/ASPE in the presence of successive additions of DA, while keeping PA at a constant concentration of 20 μM . It could be seen that the oxidation peak current for DA increased consistently with its concentration, while the peak current for PA remained unchanged (RSD = 0.95%). The corresponding calibration plot (Fig. 8B) reveals two distinct linear regions: the first from 1.0 to 70 μM and the second from 70 to 200 μM , with linear correlation coefficients of 0.995 and 0.994, respectively. The regression equations for these regions are as follows: $I_p (\mu A) = 0.158 C_{DA} (\mu M) + 7.83$ and $I_p (\mu A) = 0.051 C_{DA} (\mu M) + 14.9$.

Similarly, when the concentration of DA was fixed at 20 μM and PA was varied (Fig. 8C), the value of I_p for PA increased regularly with its concentration, while the value of I_p for DA remained constant (RSD = 1.8%). Fig. 8D illustrates two distinct linear relationships between the oxidation current and PA concentration. The first linear range extends from 1.0 to

100 μM , while the second extends up to 330 μM . The corresponding linear regression equations for these concentration ranges are:

$I_p (\mu\text{A}) = 0.085 C_{\text{PA}} (\mu\text{M}) + 4.53$ ($R^2 = 0.991$) and $I_p (\mu\text{A}) = 0.035 C_{\text{PA}} (\mu\text{M}) + 8.991$ ($R^2 = 0.997$), respectively.

Based on the first linear range, the sensitivity and limits of detection were determined as $1.93 \mu\text{A} \mu\text{M}^{-1} \text{cm}^{-2}$ and $0.11 \mu\text{M}$ for DA, and $1.06 \mu\text{A} \mu\text{M}^{-1} \text{cm}^{-2}$ and $0.17 \mu\text{M}$ for PA. These results demonstrate that SWV can effectively quantify PA and DA without any loss in peak current intensity.

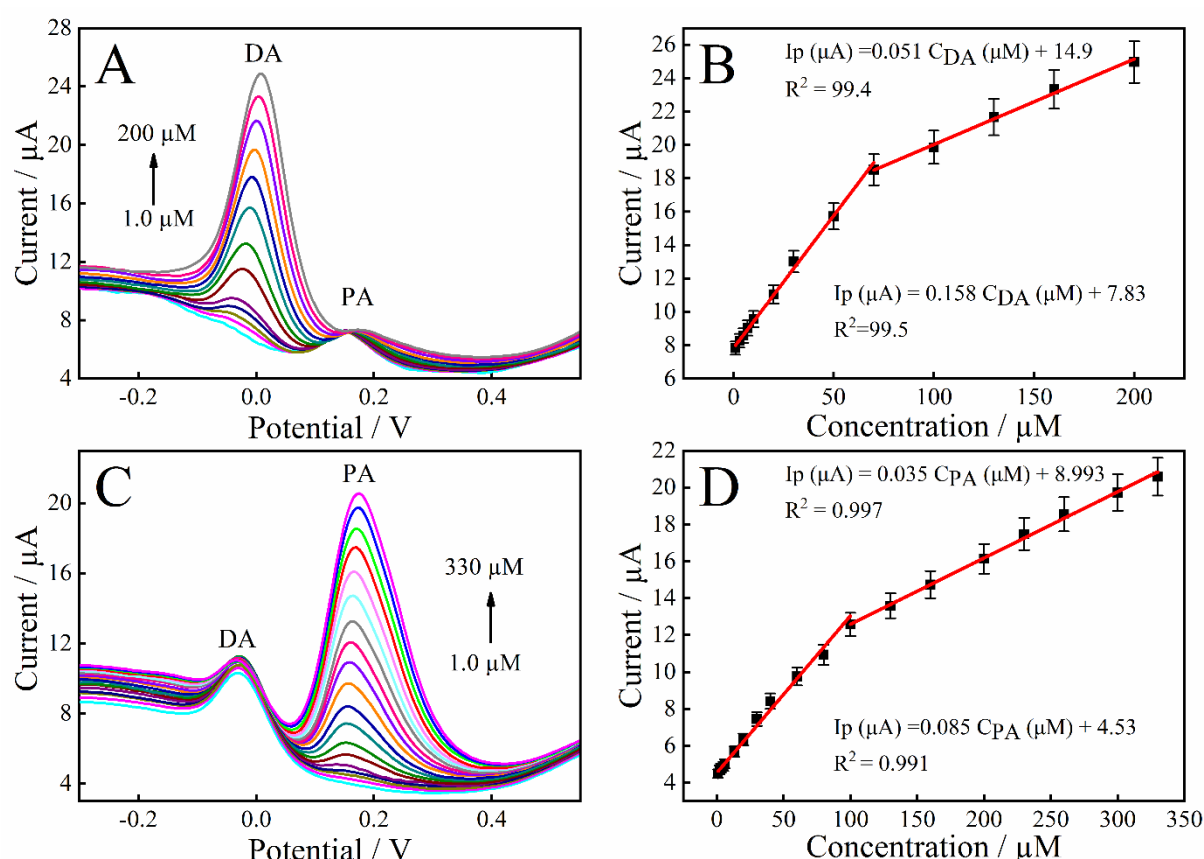


Fig. 8 SWVs response of various concentrations of (A) DA, (C) PA, at RuNPs/ASPE in 0.1 M PBS, scan rate 50 mV s^{-1} ; (B, D) show the plot of I_{pa} vs. concentration of DA and PA.

This study aimed to demonstrate the ability to simultaneously identify electroactive species of biologically and pharmaceutically important compounds. To assess sensitivity and response, CV and SWV measurements were conducted using RuNPs/ASPE while simultaneously varying the concentrations of both target analytes. Fig. 9A shows the CVs of simultaneously increasing concentrations DA and PA in 0.1 M PBS at pH 7.4. The current peak of DA was clearly separated from that of PA, their oxidation peak currents also increased, and good linear relationships were observed.

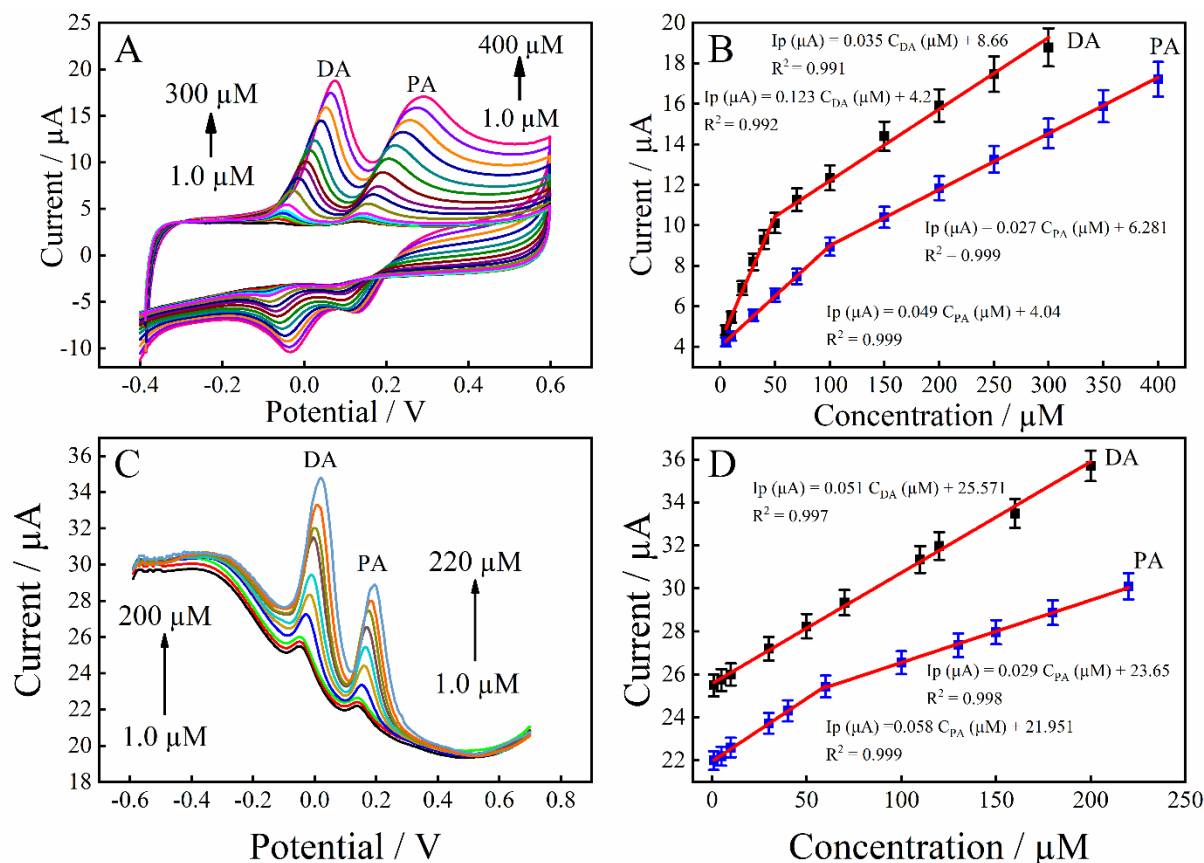


Fig. 9 (A) CVs curves of RuNPs/ASPE at various concentrations of DA (1–300 μM) and PA (1–400 μM) in 0.1 M PBS (pH 7.4) at scan rate 50 mV s⁻¹; (B) Calibration curves of current vs. DA and PA concentrations; (C) SWVs at RuNPs/ASPE with various concentrations of DA (1–200 μM) and PA (1–220 μM) in 0.1 M PBS (pH 7.4) at scan rate 50 mV s⁻¹; (D) plots of I_{pa} vs. DA and PA concentration.

The dynamic linear calibration curve exhibited two distinct regions for each analyte (Fig. 9B). For dopamine, the linear equations were $I_p (\mu A) = 0.123 C_{DA} (\mu M) + 4.268$ in the range of 1.0–50 μM ($R^2 = 0.992$) and $I_p (\mu A) = 0.035 C_{DA} (\mu M) + 8.666$ in the range of 50–200 μM ($R^2 = 0.991$). Similarly, for paracetamol, the linear equations were $I_p (\mu A) = 0.049 C_{PA} (\mu M) + 4.04$ in the range of 1.0–100 μM ($R^2 = 0.999$) and $I_p (\mu A) = 0.027 C_{PA} (\mu M) + 6.282$ in the range of 100–400 μM ($R^2 = 0.999$). The sensitivity and LODs were determined as 1.5 μA μM⁻¹ cm⁻² and 1.0 μM for DA, and 0.61 μA μM⁻¹ cm⁻² and 1.2 μM for PA. Consistent with the previous CV results, the linear ranges, LODs, and sensitivity of the RuNPs/ASPE were evaluated during the simultaneous determination of DA and PA using SWV.

As shown in Fig. 9C, the oxidation peak currents of both molecules progressively increase with concentration, demonstrating strong linearity between concentration and peak current.

The calibration curves for DA and PA (Fig. 9D) exhibited good linear relationships within the given concentration ranges, as described by the following linear regression equations: $I_p (\mu A) = 0.051 C_{DA}(\mu M) + 25.571$ (1–200 μM , $R^2 = 0.997$) for DA, and $I_p (\mu A) = 0.058 C_{PA} (\mu M) + 21.951$ (1–60 μM , $R^2 = 0.999$), $I_p (\mu A) = 0.029 C_{PA} (\mu M) + 23.65$ (60–220 μM , $R^2 = 0.998$), for PA. The sensitivity and LODs were estimated as $0.65 \mu A \mu M^{-1} cm^{-2}$ and $0.84 \mu M$ for DA, and $0.72 \mu A \mu M^{-1} cm^{-2}$ and $0.75 \mu M$ for PA, respectively. Table 1 compares the novel RuNPs/ASPE sensor to other previously described sensors in the literature for DA and PA detection. Thus, our newly RuNPs/ASPE displayed excellent performance, with suitable linear ranges and a lower detection limit for both analytes, compared to some noble metal modified electrodes.

Table 1 Performance comparison of different electrodes for the detection of DA and PA.

Modified electrode	Method	Linear range/ μM		Detection limit/ μM		Ref
		DA	PA	DA	PA	
ZIF-67 ^a	DPV	2–45	2–45	1.3	1.4	[56]
3DRGO/MWNCTs@ZrFeOx/GCE ^b	DPV	1–180	1–190	0.23	0.212	[21]
Fe ₂ O ₃ /CPE ^c	DPV	2–170	2–150	0.79	1.16	[57]
NiO–CuO/GR/GCE ^d	DPV	0.5–20	4–400	0.17	1.33	[58]
3DIPC-IL/CS/GCE ^e	DPV	1–500	1–700	0.13	0.58	[59]
MnFe ₂ O ₄ /GP ^f	DPV	5–200	3–160	0.4	0.3	[60]
CoFe ₂ O ₄ /GP ^g	DPV	3–180	3–200	0.35	0.25	
f-MWCNTs/GCE ^h	DPV	3–200	3–300	0.8	0.6	[61]
CB-PAH/GCE ⁱ	LSV	1–22	2.4–27	0.55	1.3	[62]
GCE/Cu ²⁺ @PDA-MWCNTs ^j	DPV	4–125	5–75	0.87	0.92	[63]
RuNPs/ASPE	CV	1–300	1–400	0.8	0.7	This work
	SWV	1–200	1–330	0.11	0.17	

^a ZIF-67: Zeolitic imidazolate framework – 67

^b 3D: three-dimensional structure; RGO: reduced graphene oxide; MWNCTs: multi-wall carbon nanotubes; ZrFeOx: bimetallic-organic gel; GCE: glassy carbon electrode

^c Fe₂O₃: iron oxide nanoparticle; CPE: carbon paste electrode

^d NiO: nickel oxide nanoparticles ; CuO: copper oxide nanoparticles; GR: graphene

^e 3DIPC-IL: three-dimensional interconnected porous carbon-ionic liquid ;CS : chitosan

^f MnFe₂O₄ : manganese ferrite; GP: graphite

^g CoFe₂O₄ : cobalt ferrite

^h f-MWCNTs: acid functionalized multi-wall carbon nanotubes

ⁱ CB: carbon black ; PAH: poly(allylamine hydrochloride) film

^j Cu²⁺ : copper ; PDA polydopamine complex

2.7 Selectivity, reproducibility, and stability of the sensor

The stability, selectivity, and repeatability of the RuNPs/ASPE sensor were evaluated using SWV under optimal experimental conditions. Repeatability was assessed by performing five consecutive measurements in 0.1 M PBS containing 100 μM DA and PA (Figs.S5A and S5B). The obtained relative standard deviations (RSDs) were 0.85% for DA and 1.12% for PA, demonstrating that the modified sensor resists surface fouling from oxidation products and is

suitable for repeated consecutive measurements. The reproducibility of the RuNPs/ASPE sensor was assessed by detecting 100 μ M DA and 100 μ M PA in 0.1 M PBS using five independently fabricated electrodes (Figs. S5C and S5D). The RSD values were 1.94% for DA and 2.58% for PA, confirming the excellent reproducibility of the developed sensor. Finally, the stability of the functionalized RuNPs/ASPE electrode was evaluated after eight weeks of storage at ambient temperature. The current responses for DA and PA were compared before and after storage (Figs. S5E and S5F). The results showed that the catalytic current retained 91% of its initial value, demonstrating the electrode's long-term stability. The excellent reproducibility and stability of the sensor can be attributed to the unique structural properties of the RuNPS/ASPE.

2.8 Interference studies

This study aimed to evaluate the performance of the RuNPS/ASPE sensor for detecting DA and PA simultaneously in the presence of higher concentration of AA and UA. Due to their similar structures and oxidation potentials, AA and UA can interfere with the electrochemical detection of DA and PA, particularly in biological systems where these compounds coexist, complicating selective and accurate detection. Fig. 10A shows the SWV curves of the mixed solutions of DA (100 μ M), PA (100 μ M), UA (500 μ M) and AA (500 μ M). As shown in this figure, the addition of AA and UA to the solution containing DA and PA results in a positive shift in the oxidation peaks of both PA and DA. The oxidation potentials of the four compounds are -0.26 V (AA), 0.01 V (DA), 0.2 V (PA), and 0.52 V (UA), respectively. These results indicate that the modified RuNPS/ASPE does not interfere with the current response for DA and PA detection in the presence of AA and UA. Moreover, the oxidation peak of UA on the RuNPS/ASPE electrode appears after that of PA, in contrast to other studies where the UA oxidation peak lies between those of DA and PA, very close to that of paracetamol [21]. This result demonstrates that our sensor is highly selective in detecting DA and PA simultaneously in the presence of AA and UA.

In addition to AA and UA, other common interferents that typically coexist with DA and PA in human blood serum or pharmaceutical samples were evaluated using SWV. Known concentrations of key organic interferents, including glucose, caffeine, sucrose, and fructose, as well as inorganic species such as NaCl, CaCO₃, and KNO₃, were introduced into the analytical solution containing 20 mM DA and 20 mM PA (pH 7.4 PBS). Fig. 10B shows minimal variation in the peak current (I_p) for all analytes. The results suggested that the RuNPS/ASPE had good selectivity and anti-interference abilities.

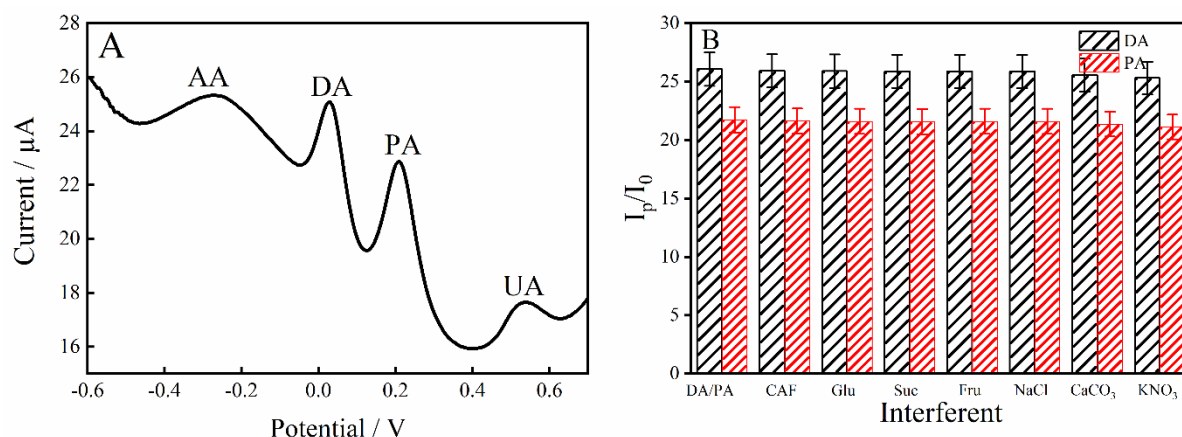


Fig.10 (A) Interference of RuNPs/ASPE sensor in the presence of 100 μM DA, 100 μM PA, 500 μM AA, and 500 μM UA; (B) Bar diagram of peak current (I_p) for DA and PA concentrations with and without interfering biomolecules and salts.

2.9 Feasibility Assessment in Pharmaceutical and Blood Samples

The feasibility of the RuNPs/ASPE was further assessed by analyzing identical concentrations of PA and DA in commercial pharmaceutical samples, including injectable dopamine solutions (40 mg/mL) and paracetamol tablets (1000 mg/tablet), as well as in standard buffer solutions. Measurements were performed under optimized conditions using the SWV technique. The sample pre-treatment method is described in detail in Section 1.4

As shown in Figs. 11A and 11B, the newly developed sensor exhibited comparable current responses in both cases, demonstrating its suitability for practical applications.

The results, summarized in Table 2, closely matched the manufacturer's specified target contents, with recovery rates ranging from 98.02% to 103.84%.

Furthermore, the RSD values for each sample, based on three parallel measurements, remained below 3.26%. Notably, tablet additives did not interfere with analyte detection in commercial samples. These findings confirm that the developed RuNPs/ASPE sensor is both reliable and accurate for determining DA and PA in pharmaceutical samples.

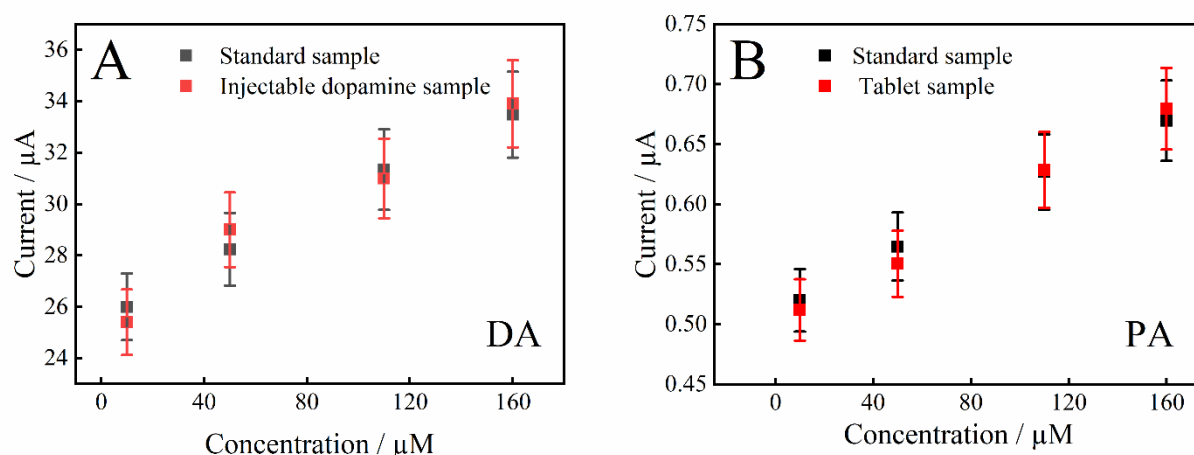


Fig. 11 Sensor responses for the same analyte concentrations in injectable dopamine samples (A) and tablet samples (B) compared to standard solutions.

Table 2

Determination of DA and PA by RuNPs/ASPE in dopamine hydrochloride injection and in pharmaceutical tablet (n=3).

Pharmaceutical preparation	Sample	Reported content		Determined		Recovery (%)		RSD (%)	
		DA	PA	DA	PA	DA	PA	DA	PA
Dopamine hydrochloride injection (mg/ml)	1	20	–	20.76±0.17	ND	103.84	–	1.58	–
	2	40	–	40.66±0.64	ND	101.65	–	1.34	–
Paracetamol tablet (mg)	1	–	500	ND	490.1±84	–	98.02	–	2.04
	2	–	1000	ND	992.9±0.76	–	99.29	–	3.26

ND: not detected

Furthermore, recovery tests for the simultaneous detection of DA and PA in human blood samples were performed under identical conditions using the SWV technique. The analyses involved the individual addition of 2.0 and 4.0 μM of DA, and 10 and 100 μM of PA to human blood samples. As summarized in Table 3, the recovery rates ranged from 97.37% to 102.27%, with RSD values below 3%. These results highlight the strong potential of the modified RuNPs/ASPE sensor for the accurate and reliable simultaneous detection of DA and PA in real serum samples.

Table 3

Determination of mixtures of DA and PA in human serum samples (n=3).

Sample	Analyte (μM)				Recovery (%)		R.S.D.(%)	
	Added		Found					
	DA	PA	DA	PA	DA	PA	DA	PA
Serum 1	–	–	0.97 ± 0.48	21.6 ± 0.22	–	–	1.45	1.63
Serum 2	2	50	3.05 ± 0.83	72.54 ± 0.45	97.37	98.71	1.89	2.01
Serum 3	4	100	5.07 ± 0.71	118.9 ± 0.68	98.02	102.27	2.1	2.98

3. Conclusion

In this work, we have successfully developed electrochemically activated graphite SPEs decorated with Ru nanoparticles using a simple electrochemical route based on the CV method. The surface and chemical morphology of the as-prepared materials were thoroughly examined. The RuNPs/ASPE electroactivity was evaluated for the electrooxidation of DA and PA using CV, EIS and SWV methods. For individual detection, SWV and EIS proved to be better techniques, particularly SWV, which exhibited the highest sensitivity and the lowest detection. However, for simultaneous detection, CV is more advantageous, providing the widest linear ranges. This excellent electrochemical performance is attributed to the high catalytic activity of Ru nanoparticles and, the porous structure of activated graphite. Additionally, the surface functional groups existing in activated graphite, such as phenolic, and carboxyl, which participate in the oxidation of the absorbed intermediate species formed during the dissociation of DA and PA. Furthermore, the proposed sensor showed excellent repeatability, reproducibility, long-time stability, and selectivity toward target analytes in the vicinity of interfering species. However, the presence of potential drug interfering compounds AA and UA had no effect on the voltammetric responses of DA and PA.

Finally, these results confirmed that the obtained sensor achieved excellent recovery rates for the simultaneous determination of PA and DA in both pharmaceutical and human serum samples.

CRediT authorship contribution statement

Dalia Ghediri: Conceptualization, Data curation, Formal analysis, Investigation, Methodology, Validation, Visualization, Writing – original draft. **Rafiaa Kihal:** Data curation, Formal analysis. **Mohamed Lyamine Chelaghmia:** Conceptualization, Data curation, Formal analysis, Investigation, Methodology, Supervision, Validation, Visualization, Writing – review & editing. **Abdulaziz K. Assaifan:** Data curation, Funding acquisition, Validation. **Craig E. Banks:** Data curation, Validation, Visualization. **Fatima Zahra Makhoul:** Formal analysis,

Methodology. **Hassina Fisli:** Formal analysis, Methodology. **Mouna Nacef:** Formal analysis, Supervision. **Abed Mohamed Affoune:** Formal analysis, Supervision. **Serge Mbokou Foukmeniok:** Formal analysis, **Maxime Pontié:** Formal analysis

Declaration of competing interest

The authors declare that they have no known competing financial interests or personal relationships that could have appeared to influence the work reported in this paper.

Data availability

Data will be made available on request.

Funding

The authors extend their appreciation to the King Salman center For Disability Research for funding this work through Research Group no KSRG-2024-102.

Acknowledgement

The authors extend their appreciation to the King Salman center For Disability Research for funding this work through Research Group no KSRG-2024-102. Also, the authors acknowledges the financial support within the General Direction of Scientific Research and Technology Development of the Algerian ministry of higher education and scientific research.

References

- [1]. T.T. Calam, Selective and Sensitive Determination of Paracetamol and Levodopa with Using Electropolymerized 3,5-Diamino-1,2,4-triazole Film on Glassy Carbon Electrode, *Electroanalysis* 33 (2021) 1049–1062.
- [2] S.V. Selvi, A. Krishnapandi, S.-M. Chen, A. Prasannan, P.-D. Hong, B. Arumugam, Physically stimulated carbon black combined cobalt manganese oxide: A pinpoint assessment of dopamine sensor towards human fluids, *Microchem. J.* 194 (2023) 109236.
- [3] A. Kutluay, M. Aslanoglu, An electrochemical sensor prepared by sonochemical one-pot synthesis of multi-walled carbon nanotube-supported cobalt nanoparticles for the simultaneous determination of paracetamol and dopamine, *Anal. Chim. Acta* 839 (2014) 59–66.
- [4] S. M, B.E.K. Swamy, K.A. Vishnumurthy, Iron Oxide Modified Carbon Paste Electrode Sensor for Guanine and Dopamine: A Voltammetric Technique, *Anal. Bioanal. Electrochem.* 15 (2023) 444-457.
- [5] P. Gupta, R.N. Goyal, Y.-B. Shim, Simultaneous analysis of dopamine and 5-hydroxyindoleacetic acid at nanogold modified screen printed carbon electrodes, *Sens. Actuators B Chem.* 213 (2015) 72–81.
- [6] Y. Si, Y.E. Park, J.E. Lee, H.J. Lee, Nanocomposites of poly(L -methionine), carbon nanotube–graphene complexes and Au nanoparticles on screen printed carbon electrodes for electrochemical analyses of dopamine and uric acid in human urine solutions, *Analyst* 145 (2020) 3656–3665.
- [7] C. Chen, J. Ren, P. Zhao, J. Zhang, Y. Hu, J. Fei, A novel dopamine electrochemical sensor based on a β -cyclodextrin/Ni-MOF/glassy carbon electrode, *Microchem. J.* 194 (2023) 109328.
- [8] B.G. Mahmoud, M. Khairy, F.A. Rashwan, C.E. Banks, Simultaneous Voltammetric Determination of Acetaminophen and Isoniazid (Hepatotoxicity-Related Drugs) Utilizing Bismuth Oxide Nanorod Modified Screen-Printed Electrochemical Sensing Platforms, *Anal. Chem.* 89 (2017) 2170–2178.
- [9] Y. Feng, Y. Li, S. Yu, Q. Yang, Y. Tong, B.-C. Ye, Electrochemical sensor based on N-doped carbon dots decorated with manganese oxide nanospheres for simultaneous detection of p -aminophenol and paracetamol, *Analyst* 146 (2021) 5135–5142.
- [10] T. Kokab, A. Shah, M.A. Khan, M. Arshad, J. Nisar, M.N. Ashiq, M.A. Zia, Simultaneous Femtomolar Detection of Paracetamol, Diclofenac, and Orphenadrine Using a Carbon Nanotube/Zinc Oxide Nanoparticle-Based Electrochemical Sensor, *ACS Appl. Nano Mater.* 4 (2021) 4699–4712.

- [11] J. Tang, Z.-Z. Hui, T. Hu, X. Cheng, J.-H. Guo, Z.-R. Li, H. Yu, A sensitive acetaminophen sensor based on Co metal–organic framework (ZIF-67) and macroporous carbon composite, *Rare Met.* 41 (2022) 189–198.
- [12] N.F.B. Azeredo, J.M. Gonçalves, I.S. Lima, K. Araki, J. Wang, L. Angnes, Screen-printed Nickel-Cerium Hydroxide Sensor for Acetaminophen Determination in Body Fluids, *ChemElectroChem* 8 (2021) 2505–2511.
- [13] K. Annadurai, V. Sudha, G. Murugadoss, R. Thangamuthu, Electrochemical sensor based on hydrothermally prepared nickel oxide for the determination of 4-acetaminophen in paracetamol tablets and human blood serum samples, *J. Alloys Compd.* 852 (2021) 156911.
- [14] Y. Zhang, X. Jiang, J. Zhang, H. Zhang, Y. Li, Simultaneous voltammetric determination of acetaminophen and isoniazid using MXene modified screen-printed electrode, *Biosens. Bioelectron.* 130 (2019) 315–321.
- [15] K.K. Kumar, D. M, P.S. Kumar, R.S. Babu, S.S. Narayanan, Green synthesis of curcumin-silver nanoparticle and its modified electrode assisted amperometric sensor for the determination of paracetamol, *Chemosphere* 303 (2022) 134994.
- [16] S. Bohler, X. Liu, J. Krauskopf, F. Caiment, J. Aubrecht, G.A.F. Nicolaes, J.C.S. Kleinjans, J.J. Briedé, Acetaminophen Overdose as a Potential Risk Factor for Parkinson's Disease, *Clinical Translational Sci* 12 (2019) 609–616.
- [17] C. Luhana, P. Mashazi, Simultaneous Detection of Dopamine and Paracetamol on Electroreduced Graphene Oxide–Cobalt Phthalocyanine Polymer Nanocomposite Electrode, *Electrocatalysis* 14 (2023) 406–417.
- [18] J.V.H. Ramos, F.D.M. Morawski, T.M.H. Costa, S.L.P. Dias, E.V. Benvenutti, E.W. De Menezes, L.T. Arenas, Mesoporous chitosan/silica hybrid material applied for development of electrochemical sensor for paracetamol in presence of dopamine, *Microporous Mesoporous Mater* 217 (2015) 109–118.
- [19] B. Ranjani, J. Kalaiyarasi, D.M. Soundari, K. Pandian, S.C.B. Gopinath, Synthesis of novel nanostructured copper tungstate/GCE electrochemical system in deep eutectic solvent medium for simultaneous detection of dopamine and paracetamol, *Inorg. Chem. Commun* 145 (2022) 109879.
- [20] A. Kader Mohiuddin, M. Shamsuddin Ahmed, S. Jeon, Palladium doped α -MnO₂ nanorods on graphene as an electrochemical sensor for simultaneous determination of dopamine and paracetamol, *Appl. Surf. Sci.* 578 (2022) 152090.

- [21] A. Xie, H. Wang, J. Lin, J. Pan, M. Li, J. Wang, S. Jiang, S. Luo, 3D RGO/MWCNTs-loaded bimetallic-organic gel derived ZrFeOx as an electrochemical sensor for simultaneous detection of dopamine and paracetamol, *J. Alloys Compd.* 938 (2023) 168647.
- [22] X. Zhou, Y. Kuang, J. Li, S. Hu, C. Cheng, J. Wang, X. Qin, L. Ou, Z. Su, Melamine-Based nanocomposites for selective dopamine and uric acid sensing, *ACS Appl. Polym. Mater.* 5, 7 (2023) 5609–5619.
- [23] X. Liu, E. Shangguan, J. Li, S. Ning, L. Guo, Q. Li, A novel electrochemical sensor based on FeS anchored reduced graphene oxide nanosheets for simultaneous determination of dopamine and acetaminophen, *Mater. Sci. Eng. C* 70 (2017) 628–636.
- [24] W. Boumya, M. Achak, M. Bakasse, M.A. El Mhammedi, Indirect determination of dopamine and paracetamol by electrochemical impedance spectroscopy using azo coupling reaction with oxidized 2,4-dinitrophenylhydrazine (DNPH): Application in commercial tablets, *J. Sci: Adv. Mater. Devices* 5 (2020) 218–223.
- [25] Z. Su, Y. Liu, Q. Xie, L. Chen, Y. Zhang, Y. Meng, Y. Li, Y. Fu, M. Ma, S. Yao, Preparation of thiolated polymeric nanocomposite for sensitive electroanalysis of dopamine, *Biosens. Bioelectron.* 36 (2012) 154–160
- [26] S. Abdi, M.L. Chelaghmia, R. Kihal, C.E. Banks, A.G.M. Ferrari, H. Fisli, M. Nacef, A.M. Affoune, M.E.H. Benhamza, Simultaneous determination of 4-aminophenol and paracetamol based on CS-Ni nanocomposite-modified screen-printed disposable electrodes, *Monatsh Chemie* 154 (2023) 563–575.
- [27] M.L. Chelaghmia, H. Fisli, M. Nacef, D.A.C. Brownson, A.M. Affoune, H. Satha, C.E. Banks, Disposable non-enzymatic electrochemical glucose sensors based on screen-printed graphite macroelectrodes modified via a facile methodology with Ni, Cu, and Ni/Cu hydroxides are shown to accurately determine glucose in real human serum blood samples, *Anal. Methods* 25 (2021) 2812–2822.
- [28] K. Torres-Rivero, A. Florido, J. Bastos-Arrieta, Recent Trends in the Improvement of the Electrochemical Response of Screen-Printed Electrodes by Their Modification with Shaped Metal Nanoparticles, *Sensors* 21 (2021) 2596.
- [29] M.Z. Abedeen, M. Sharma, H. Singh Kushwaha, R. Gupta, Sensitive enzyme-free electrochemical sensors for the detection of pesticide residues in food and water, *TrAC. Trends Anal. Chem.* 176 (2024) 117729.
- [30] J.P. Metters, R.O. Kadara, C.E. Banks, New directions in screen printed electroanalytical sensors: an overview of recent developments, *Analyst* 136 (2011) 1067.

- [31] Z. Liang, S. Hu, Y. Peng, C. Cheng, J. Luo, L. Yang, M. Yang, X. Yu, Y. Zhao, Z. Su, A Smart portable sensor with ratio and dual-mode for in situ detection of nicotine in tobacco leaves, *IEEE Sens. J.* 24 (2024) 71–77.
- [32] Z. Su, S. Hu, Y. Zhang, Z. Liang, Y. Peng, Q. Cao, X. Yu, Z. Zhu, P. He, Z. Li, Electrodeposition of paracetamol oxide for intelligent portable ratiometric detection of nicotine and ethyl vanillin β -d-glucoside *Analyst*, 149 (2024) 188–195
- [33] Z. Su, S. Hu, Y. Xu, J. Liu, P. Liang, J. Wang, Q. Cao, Y. Peng, W. Zhang, D. Fan, A smart portable electrochemical sensor based on electrodeposited ferrocene-functionalized multiwalled carbon nanotubes for in vitro and in vivo detection of nicotine in tobacco samples, *New J. Chem.* 48 (2024) 3370–3380.
- [34] E.P. Randviir, D.A.C. Brownson, J.P. Metters, R.O. Kadara, C.E. Banks, The fabrication, characterisation and electrochemical investigation of screen-printed graphene electrodes, *Phys. Chem. Chem. Phys.* 16 (2014) 4598–4611.
- [35] A.A. Khorshed, M. Khairy, C.E. Banks, Electrochemical determination of antihypertensive drugs by employing costless and portable unmodified screen-printed electrodes, *Talanta* 198 (2019) 447–456.
- [36] J. Kozak, K. Tyszczyk-Rotko, M. Wójciak, I. Sowa, M. Rotko, First Screen-Printed Sensor (Electrochemically Activated Screen-Printed Boron-Doped Diamond Electrode) for Quantitative Determination of Rifampicin by Adsorptive Stripping Voltammetry, *Materials* 14 (2021) 4231.
- [37] A. Jirasirichote, E. Punrat, A. Suea-Ngam, O. Chailapakul, S. Chuanuwatanakul, Voltammetric detection of carbofuran determination using screen-printed carbon electrodes modified with gold nanoparticles and graphene oxide, *Talanta* 175 (2017) 331–337.
- [38] P. Cervini, I.A. Mattioli, É.T.G. Cavaleiro, Developing a screen-printed graphite–polyurethane composite electrode modified with gold nanoparticles for the voltammetric determination of dopamine, *RSC Adv.* 9 (2019) 42306–42315.
- [39] F.Z. Makhoul, M.L. Chelaghmia, R. Kihal, C.E. Banks, H. Fisli, M. Nacef, A.M. Affoune, M. Pontié, Screen-printed electrodes decorated with low content Pt–Ni microstructures for sensitive detection of Zn(II), ascorbic acid and paracetamol in pharmaceutical products and human blood samples, *Microchem. J.* 206 (2024) 111467.
- [40] S. Palanisamy, B. Thirumalraj, S.-M. Chen, M.A. Ali, F.M.A. Al-Hemaid, Palladium nanoparticles decorated on activated fullerene modified screen printed carbon electrode for enhanced electrochemical sensing of dopamine, *J. Colloid Interface Sci.* 448 (2015) 251–256.

- [41] S. Redžića, E. Kahrovićb, A. Zahirovićb, E. Turkušićb, Electrochemical Determination of Dopamine with Ruthenium (III)-Modified Glassy Carbon and Screen-Printed Electrodes, *Anal. Lett.* 50 (2017) 1602–1619.
- [42] J. Hafeez, M. Bilal, N. Rasool, U. Hafeez, S. Adnan Ali Shah, S. Imran, Z. Amiruddin Zakaria, Synthesis of ruthenium complexes and their catalytic applications: A review, *Arab. J. Chem.* 15 (2022) 104165.
- [43] D. Boglaienko, G.B. Hall, N.L. D’Annunzio, T.G. Levitskaia, Ruthenium speciation and distribution in the environment: A review, *Sci. Total Environ.* 951 (2024) 175629.
- [44] A.M. Asran, M.A. Mohamed, G.M.G. Eldin, R.K. Mishra, A. Errachid, Self-assembled ruthenium decorated electrochemical platform for sensitive and selective determination of amisulpride in presence of co-administered drugs using safranin as a mediator, *Microchem. J.* 164 (2021) 106061.
- [45] M. Liu, T. Zhe, F. Li, L. Zhu, S. Ouyang, L. Wang, An ultrasensitive electrochemical sensor based on NiFe-LDH-MXene and ruthenium nanoparticles composite for detection of nitrofurantoin in food samples, *Food Chem.* 461 (2024) 140915.
- [46] M. Ikram, A. Munawar, A.A. Kalyar, N.A. Shad, M. Imran, Ruthenium decorated V@WO₃ nanocomposites heterostructures for selective detection of sulfonamide in honey samples, *J. Food Compos. Anal.* 126 (2024) 105842.
- [47] K. Prabhu, S. J. Malode, N. P. Shetti, S. Pandiaraj, A. Alodhayb, M. Muthuramamoorthy Determination of fungicide at Ru-doped TiO₂/reduced graphene oxide decorated electrochemical sensor, *Microchem. J.* 197 (2024) 109722.
- [48] M. Duraisamy, M. Elanchezian, M. Eswaran, S. Ganesan, A.A. Ansari, G. Rajamanickam, S.L. Lee, P.-C. Tsai, Y.-H. Chen, V.K. Ponnusamy, Novel ruthenium-doped vanadium carbide/polymeric nanohybrid sensor for acetaminophen drug detection in human blood, *Int. j. Boil. Macromol* 244 (2023) 125329.
- [49] A.A. Abdelwahab, A.H. Naggat, M. Abdelmotaleb, M.Y. Emran, Ruthenium Nanoparticles Uniformly-designed Chemically Treated Graphene Oxide Nanosheets for Simultaneous Voltammetric Determination of Dopamine and Acetaminophen, *Electroanalysis* 32 (2020) 2156–2165.
- [50] W. Drissi, M.L. Chelaghmia, M. Nacef, A.M. Affoune, H. Satha, R. Kihal, H. Fisli, C. Boukharouba, M. Pontié, In situ growth of Ni(OH)₂ nanoparticles on 316L stainless steel foam: an efficient three-dimensional non-enzymatic glucose electrochemical sensor in real human blood serum samples, *Electroanalysis* 34 (2022) 1735–1744.

- [51] A. G. M. Ferrari, C. W. Foster, P. J. Kelly, D. A. C. Brownson, C. E. Banks, Determination of the Electrochemical Area of Screen-Printed Electrochemical Sensing Platforms, *Biosensors*, 8 (2018) 53–63.
- [52] M.L. Chelaghmia, M. Nacef, A.M. Affoune, Ethanol electrooxidation on activated graphite supported platinum–nickel in alkaline medium, *J. Appl. Electrochem.* 42 (2012) 819–826.
- [53] T. Kokab, A. Shah, M. A. Khan, M. Arshad, J. Nisar, M. N. Ashiq, M. A. Zia, Simultaneous Femtomolar Detection of Paracetamol, Diclofenac, and Orphenadrine Using a Carbon Nanotube/Zinc Oxide Nanoparticle-Based Electrochemical Sensor, *ACS Appl. Nano Mater.* 5 (2021) 4699–4712.
- [54] M. Achache, G. E. Idrissi, N. Ben Seddik, S. El Boumlasy, I. Kouda, I. Raissouni, F. Chaouket, K. Draoui, D. Bouchta, M. Choukairi, Innovative use of shrimp shell powder in carbon paste electrode for the electrochemical detection of dopamine and paracetamol: Valorization, characterization and application, *Microchem. J.* 202 (2024) 110754.
- [55] M. Emadoddin, S. A. Mozaffari, F. Ebrahimi, An antifouling impedimetric sensor based on zinc oxide embedded polyvinyl alcohol nanoplatelets for wide range dopamine determination in the presence of high concentration ascorbic acid; *J. Pharm. Biomed. Anal.* 205, (2021) 114278.
- [56] N.T.T. Tu, P.C. Sy, T.V. Thien, et al., Microwave-assisted synthesis and simultaneous electrochemical determination of dopamine and paracetamol using ZIF-67-modified electrode, *J. Mater. Sci.* 54 (2019) 11654–11670.
- [57] M.M. Vinay, Y.Arthoba Nayaka, Iron oxide (Fe_2O_3) nanoparticles modified carbon paste electrode as an advanced material for electrochemical investigation of paracetamol and dopamine, *J. Sci. -Adv. Mater. Dev.* 4 (2019) 442–450.
- [58] B. D Liu, X.Q. Ouyang, Y.P. Ding, et al., Electrochemical preparation of nickel and copper oxides decorated graphene composite for simultaneous determination of dopamine, acetaminophen and tryptophan, *Talanta* 146 (2016) 114–121.
- [59] X. Kang , Y. Song, J. Zhao, Y. Li, Simultaneous determination of paracetamol and Dopamine, and detection of bisphenol a using Three-dimensional interconnected porous carbon functionalized with ionic liquid, *J. Electroanal. Chem.* 895 (2021) 115482.
- [60] Y. Kumar, P. Pramanik, D.K. Das, Electrochemical detection of paracetamol and dopamine molecules using nano-particles of cobalt ferrite and manganese ferrite modified with graphite, *Heliyon* 5 (2019) e02031.

- [61] Z.A. Allothman, N. Bukhari, S.M. Wabaidur, S. Haider, Simultaneous electrochemical determination of dopamine and acetaminophen using multiwall carbon nanotubes modified glassy carbon electrode, *Sens. Actuators B Chem.* 146 (2010) 314–320.
- [62] J. Scremin, G.J. Mattos, R.D. Crapnell, S.J. Rowley-Neale, C.E. Banks, E.R. Sartori, Glassy Carbon Electrode Modified with Layering of Carbon Black/Poly(Allylamine Hydrochloride) Composite for Multianalyte Determination, *Electroanalysis* 33 (2021) 526–536.
- [63] M. Shahbakhsh, M. Noroozifar, Copper polydopamine complex/multiwalled carbon nanotubes as novel modifier for simultaneous electrochemical determination of ascorbic acid, dopamine, acetaminophen, nitrite and xanthine, *J Solid State Electrochem.* 22 (2018) 3049–3057.